

Exploring Multiple High-Scoring Subspaces in Generative Flow Networks

Xuan Yu¹ Xu Wang^{* 1 2} Rui Zhu¹ Yudong Zhang^{1 2} Yang Wang^{* 1 2 3}

Abstract

As a probabilistic sampling framework, Generative Flow Networks (GFlowNets) show strong potential for constructing complex combinatorial objects through the sequential composition of elementary components. However, existing GFlowNets often suffer from excessive exploration over vast state spaces, leading to oversampling of low-reward regions and convergence to suboptimal distributions. Effectively biasing GFlowNets toward high-reward solutions remains a non-trivial challenge. In this paper, we propose CMAB-GFN, which integrates a combinatorial multi-armed bandit (CMAB) framework with GFlowNet policies. The CMAB component prunes low-quality actions, yielding compact high-scoring subspaces for exploration. Restricting GFNs to these compact high-scoring subspaces accelerates the discovery of high-value candidates, while the exploration of different subspaces ensures that diversity is not sacrificed. Experimental results on multiple tasks demonstrate that CMAB-GFN generates higher-reward candidates than existing approaches.

1. Introduction

Generative Flow Networks (GFlowNets) (Bengio et al., 2021; Zhang et al., 2022; Cretu et al., 2024) have shown their impressive potential in generating diverse and high-scoring candidates across various domains, especially in generating combinatorial objects (Zhang et al., 2023b;a). By unifying MDPs’ sequential dynamics with flow-based probability matching, GFlowNets synthesize action trajectories that sample candidates proportionally to the desired reward distribution.

Despite this appealing objective, practical GFlowNet train-

¹University of Science and Technology of China (USTC), Hefei, China ²Suzhou Institute for Advanced Research, USTC, Suzhou, China ³State Key Laboratory of Precision and Intelligent Chemistry, USTC, Hefei, China. Correspondence to: Xu Wang <wx309@ustc.edu.cn>, Yang Wang <angyan@ustc.edu.cn>.



Figure 1. Illustration of action pruning. The triangle means initial state, the circles denote interior states, and the squares denote the terminal states. By pruning low-scoring actions (blue edges), candidates with low rewards (blue nodes) are masked. Candidates with high rewards (Orange ones) are more likely to be explored, addressing the over-exploration of low-reward candidates.

ing often suffers from inefficient exploration in large combinatorial spaces (Kim et al., 2023; Shen et al., 2023). In many realistic tasks, the vast majority of states yield negligible reward, while high-reward candidates occupy a vanishingly small fraction of the space. As a result, early and mid-stage training frequently resembles near-uniform exploration over actions, causing most sampled trajectories to terminate in low-value regions. Under limited sampling budgets, this leads to slow discovery of high-reward modes and empirical terminal distributions that underrepresent the most valuable solutions, even when the theoretical objective is reward-proportional sampling.

Several approaches attempt to increase the *greediness* of GFlowNets, thus biasing to high-reward regions. Temperature scaling modifies the target distribution to $R(x)^\beta$ with $\beta \gg 1$, but choosing β introduces instability and risks mode collapse (Malkin et al., 2022a; Lau et al., 2024). Other methods incorporate Q-values (Lau et al., 2024), local search (Kim et al., 2023), or evolutionary strategies (Kim et al., 2024a), which bias sampling toward promising regions. However, these techniques typically operate at the *local action level* and pay more attention to exploiting observed high-value regions. Once certain actions are deemed low-value, they are rarely revisited. This may irreversibly suppress actions that appear weak early but are essential for later high-reward compositions. Consequently, exploration can become trapped in a narrow region of the space.

Inspired by existing works, we observe that in structured generative domains certain actions are consistently more promising than others. For example, in molecule design, combining specific blocks tends to yield high-scoring candi-

dates more frequently. This suggests a different perspective on exploration: rather than searching uniformly over the entire state space, one may instead search over *subspaces induced by subsets of actions*. This motivates a key intuition that even after aggressively pruning actions, the remaining subspace is still vast, yet may contain a much higher density of high-reward candidates. As shown in Fig. 1, by pruning low-quality actions and retaining promising ones, we can substantially improve sampling efficiency. Based on this, we reformulate GFlowNet exploration as a *higher-level combinatorial decision problem*. Instead of sampling over the full action space at all times, we repeatedly select promising subsets of state-independent actions that define compact, high-scoring subspaces, and train the GFlowNet within those subspaces. Exploration thus occurs at the subspace level rather than solely at the trajectory level.

Formally, we define the pruning process as selecting K actions from a total of N actions to retain, thereby inducing a subspace of the original state space. Different pruning choices correspond to different subspaces, some of which contain significantly denser clusters of high-reward candidates. Importantly, our objective is not to identify a single optimal subspace, but to discover diverse high-scoring subspaces for exploration. Continuously sampling from the same subspace would inevitably increase the similarity of generated candidates, quantitative evidence for this effect is provided in the experiments.

However, identifying such promising subspaces is non-trivial. When K scales with N , the number of possible pruning configurations grows combinatorially as $\binom{N}{K}$, rendering exhaustive search infeasible. Under a limited sampling budget, the problem naturally exhibits an exploration-exploitation trade-off: one must decide whether to exploit pruning strategies that have yielded high rewards so far, or to explore alternative pruning configurations that may uncover even better subspaces. This setting can be viewed through the lens of a multi-armed bandit (MAB) problem, where each arm corresponds to an action and rewards are observed only through downstream sampling (Robbins, 1952). Since each pruning decision involves selecting a subset of actions rather than a single action, the problem more precisely aligns with the combinatorial multi-armed bandit (CMAB) framework (Chen et al., 2013), where the learner selects combinations of base arms and receives bandit feedback on the resulting base arms. We combine a CMAB framework with GFlowNets, and introduce CMAB-GFN. By considering actions as base arms in the CMAB problem, we can utilize the CMAB algorithm to select actions that are more likely to lead to high-reward candidates.

Considering that existing works (Kim et al., 2023; Shen et al., 2023) that increase GFlowNet greediness through local value thresholding often suffer from exploration col-

lapse, our method does not rely on local value thresholding to restrict actions. Instead, we partition the original search space into subspaces defined by super arms and explore them under a CMAB framework. These subspaces are continuously cycled and re-evaluated, ensuring that no region becomes persistently inaccessible. Furthermore, our algorithm explicitly enforces subspace-level exploration, preventing the sampler from collapsing into a single high-scoring subspace. Conceptually, this reflects a shift in perspective: rather than operating directly over the entire state space, we view GFlowNet sampling as a process of discovering high-reward subspaces among a large collection of candidates. This formulation naturally balances exploration and exploitation at the subspace level, avoiding the effective lock-in behavior induced by hard thresholding, and leading to more robust performance.

We evaluate the proposed CMAB-GFN on several popular tasks used in prior works, including molecule design (Bengio et al., 2021), three RNA design tasks (Sinai et al., 2020) and bit sequence task (Malkin et al., 2022a). The result demonstrates that the proposed method discovers more high-reward candidates and converges faster than baselines. Our main contributions are:

- ❶ We propose a new perspective that views GFlowNet exploration as a combinatorial search over action-induced subspaces rather than uniform exploration of the full state space.
- ❷ A novel framework CMAB-GFN is proposed, which integrates combinatorial multi-armed bandits with GFlowNet training to adaptively select high-value subspaces.
- ❸ We demonstrate through extensive experiments that CMAB-GFN substantially improves high-reward mode discovery across molecular, RNA, and synthetic sequence design tasks.

2. Related Work

GFlowNets: Since their introduction by Bengio et al. (2021), GFlowNets have advanced rapidly in theory and applications, with recent works establishing connections to variational inference (Malkin et al., 2022b), distributional analysis (Silva et al., 2025), proxy-free training in offline settings (Chen et al., 2025), and alternative loss designs (Hu et al., 2024). They have also been applied to combinatorial optimization tasks, including general problems (Zhang et al., 2023a), computation graphs (Zhang et al., 2023c), hierarchical exploration with evolutionary search (Kim et al., 2024b), and multi-objective optimization (Zhu et al., 2023). In contrast to these approaches, which mainly employ GFlowNets to solve combinatorial problems, our method leverages combinatorial optimization techniques to improve GFlowNets themselves. Complementary efforts

have enhanced GFlowNet training through Q-value integration (Lau et al., 2024), local search (Kim et al., 2023), Thompson sampling (Rector-Brooks et al., 2023), replay strategies (Vemgal et al., 2023; Shen et al., 2023), genetic and evolutionary algorithms (Kim et al., 2024a; Ikram et al., 2024), and adaptive teacher mechanisms (Kim et al., 2024c).

Combinatorial multi-armed bandit: The combinatorial multi-armed bandit (CMAB) framework was first introduced by (Chen et al., 2013). Chen et al. (2016) later extended it to nonlinear reward functions dependent on variable distributions. Subsequent work includes the cost-aware auction-based CMAB by Gao et al. (2021) and full-bandit algorithms by Agarwal et al. (2021); Fourati et al. (2024b), where no individual arm feedback is available.

3. Preliminary

In the classic Combinatorial Multi-Armed Bandit (CMAB) problem (Chen et al., 2013; 2016), there are N base arms, each associated with an unknown reward distribution. In each round, the player selects a subset of K base arms, forming a super arm, and receives a joint reward. The goal is to identify the best K arms that maximize the joint reward, which may be a non-linear function of individual arm rewards, while minimizing regret—the gap between the expected reward of always playing the optimal super arm and that of the algorithm’s choices (Chen et al., 2013; Slivkins et al., 2019; Chen et al., 2016). The central challenge lies in balancing exploration (trying diverse super arms to gather information) and exploitation (selecting the current best super arm for higher reward). Notably, the flow network embodies a similar dilemma: some regions of the state space contain dense clusters of high-reward candidates, and the algorithm must decide between probing new promising subspaces and exploiting those already identified. The feedback models of CMAB can be categorized into two types: 1) Full-bandit feedback (Chen et al., 2013; Fourati et al., 2024a), where only the aggregate reward of the played super arm is observed, and 2) Semi-bandit feedback (Chen et al., 2013; 2021), where the individual rewards of each base arm in the super arm are additionally revealed. Our problem uses *arm-level* feedback in the spirit of the semi-bandit setting: from evaluation samples, we construct per-arm statistics that guide super-arm selection. Importantly, we do *not* observe a physically separate stochastic outcome for each arm as in classical semi-bandits. Instead, arm feedback is a *proxy* derived from terminal rewards (Sec. 4.1.2).

4. Methodology

In this section, we introduce **Combinatorial Multi-Armed Bandit GFlowNet (CMAB-GFN)**, a greedy training framework designed to enhance both the quality and diversity

of generated candidates based on CMAB. Unlike prior approaches that operate over the entire flow graph (Lau et al., 2024), CMAB-GFN achieves a more balanced exploration-exploitation trade-off by selectively focusing on high-scoring subspaces of substantially reduced size.

4.1. Framework Design

4.1.1. DESIGN OF BASE AND SUPER ARMS

The core challenge in applying CMAB to GFlowNets is to define a set of base arms whose combinations (super arms) can meaningfully constrain the exploration space. A naive approach would be to treat every possible state transition $s \rightarrow s'$ as a distinct arm. However, this leads to an intractably large and state-dependent set of arms, making the CMAB problem ill-posed.

To overcome this, we observe that in many sequential generation tasks, actions can be decomposed into two components: A **state-dependent** component a_d that determines where to act (e.g., which position in a sequence to fill, which molecular stem to extend); A **state-independent** component a_i that determines what action to take, regardless of the specific state (e.g., which value to assign to a position, which building block to attach).

$$\mathcal{A}_i = \{a_i \mid (a_d, a_i) \in \mathcal{A}_s, \forall s \in \mathcal{S}\}. \quad (1)$$

\mathcal{A}_s denotes the available transitions (action set) of state s . Intuitively, \mathcal{A}_i represents the “alphabet” of primitive choices available throughout the generative process. A super arm $\mathbb{S} \subseteq \mathcal{A}_i$ is then a subset of this alphabet. By selecting a super arm, we restrict the GFlowNet policy such that at any state s , it can only take actions (a_d, a_i) where $a_i \in \mathbb{S}$. This effectively prunes all actions that use primitive choices outside \mathbb{S} . Task Examples are given in Table 1.

4.1.2. DESIGN OF REWARDS FOR BASE ARMS

We now turn to the assignment of rewards to base arms, a critical factor for ensuring stable learning. Ideally, to evaluate the quality of a base arm i , we define its expected reward as the average reward across *all* states in the entire state space that contain this base arm:

$$\mu_i = \mathbb{E}_{x \in \mathcal{X}_i} [r(x)], \quad (2)$$

where \mathcal{X}_i denotes the set of all possible states containing base arm i , and $r(x)$ is the normalized reward of state x . This definition aligns with the CMAB assumption that the reward distribution of a base arm is intrinsic to the arm itself and remains invariant across different super arms.

In practice, however, we cannot enumerate the entire state space \mathcal{X}_i due to its exponential size. Instead, we estimate the reward of base arm i using only the sampled candidates.

Table 1. Characteristics of four evaluation tasks from three perspectives.

Task	State-dependent Component (a_d)	State-independent Component (a_i , Base Arm)	\mathcal{A}_i
Bit Sequence Generation	Position to edit	Binary value to assign	$\{0, 1\}$
Molecule Design	Stem to extend	Building block to attach	Vocabulary of 105 blocks
RNA Sequence Design	Prepend or Append	Nucleotide to add	$\{A, C, G, U\}$

In the semi-bandit setting with m base arms, the reward of base arm i at round t is approximated as

$$X_i^t = \frac{1}{|C_i^t|} \sum_{x \in C_i^t} r(x), \quad (3)$$

where C_i^t denotes the set of candidates *sampled* at round t that contain base arm i , and

$$r(x) = \text{normalize}(R(x)) \quad (4)$$

is the normalized reward of candidate x with raw reward $R(x)$ from the environment. In our implementation, we use *global min–max normalization* to constrain rewards into $[0, 1]$:

$$r(x) = \text{clip}\left(\frac{R(x) - R_{\min}}{R_{\max} - R_{\min} + \epsilon}, 0, 1\right), \quad (5)$$

where R_{\min} and R_{\max} are the global minimum and maximum raw rewards observed so far (updated online during sampling), and ϵ is a small constant for numerical stability.

To ensure that our empirical estimate X_i^t converges to the true expected reward μ_i , we adopt a two-phase sampling strategy, which *asymptotically* preserves the distributional consistency required by CMAB as the flow network accumulates diverse training experience (Theorem 4.1.4):

① Constrained training. Train the flow network restricted to \mathbb{S} .

② Unrestricted evaluation. Sample candidates without restrictions, and compute X_i as the average reward over all candidates containing arm i .

This procedure increases the sampling cost but does not increase network training complexity, while asymptotically ensuring unrestricted reward estimates as the flow network accumulates diverse training experience. Moreover, the extra cost does not scale linearly with training time, since the evaluation stage of deep networks remains unaffected. With multi-threaded sampling, the overhead can be further reduced. A detailed comparison of time consumption is reported in Table 8. It is important to note that the samples generated in the unrestricted evaluation phase are used only for updating bandit statistics and are *not* included in the final evaluation metrics reported in our experiments.

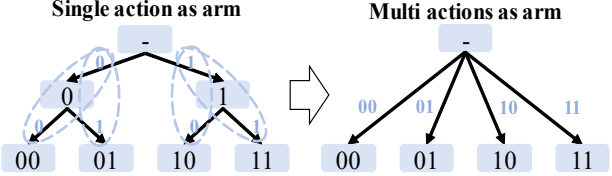


Figure 2. Using short action sequences as arms to transform the narrow-deep network architecture into a more balanced wide structure.

4.1.3. DESIGN FOR ADJUSTING NETWORK STRUCTURE

We further propose a method to address the challenge that arises when the independent action space is small but trajectories are long, resulting in narrow yet deep networks.

For instance, in bit sequence generation, there are only two independent actions, 0, 1, while a complete sequence may require over 100 steps. This leads to a deep but fragile network, where pruning even a single action can collapse the entire solution space.

To address this, we redefine base arms as short sequences of t consecutive actions:

$$a_1 \rightarrow a_2 \rightarrow \dots \rightarrow a_t.$$

Super arms then consist of sets of such sequences. A subtrajectory is valid if its independent subsequence belongs to the chosen super arm. This widens the effective search space and balances the architecture, while keeping the CMAB formulation applicable (see Fig. 2).

4.1.4. DYNAMIC NATURE OF FLOW NETWORKS

Unlike standard CMAB problems with stationary distributions, flow networks evolve during training. It is therefore important to characterize this non-stationarity. The fundamental constraint for an ideal flow network is:

$$\pi(x) = \frac{R(x)}{\sum_{x' \in \mathcal{X}} R(x')}, \quad \forall x \in \mathcal{X}, \quad (6)$$

where $\pi(x)$ represents the target distribution and $R(x)$ denotes the reward function. However, achieving this equilibrium condition requires exhaustive exploration of all states, which is impractical in real-world scenarios. Consequently, the expected rewards of individual base arms evolve dynamically throughout the training process of the flow network. Nevertheless, under a mild policy-stabilization condition (i.e., when the GFlowNet parameters eventually converge or

change sufficiently slowly), the induced arm reward distributions stabilize in late training. In our analysis, we therefore separate two aspects: (i) *TB consistency*—if the TB equations are solved (or nearly solved), the induced terminal distribution matches (or approximates) the reward-proportional target; and (ii) *training non-stationarity*—during optimization, the policy drifts, so arm reward statistics can be non-stationary. Our convergence statements below are correspondingly stated under a policy-stabilization condition, and in practice we use sliding-window estimates to track residual drift.

Theorem 1 (Convergence of Reward Distributions). Under standard regularity conditions (bounded rewards, positive exploration, appropriate learning rates, and finite state space), the reward distribution of each base arm i converges to a stable distribution as the GFlowNet policy converges. The formal statement with precise assumptions and the complete proof are provided in Appendix B.

Theorem 2 (Asymptotic Approximate Distributional Invariance). Under the two-phase protocol, if the evaluation-time conditional sampling distributions become asymptotically insensitive to which super arm was used in the preceding restricted training phase (e.g., due to diminishing policy drift / two-time-scale updates), then the arm-level reward statistics used by CMAB become approximately invariant across super arm selections in late training. The formal condition and proof are provided in Appendix B.

4.1.5. CUCB ALGORITHM FOR CMAB-GFN

We integrate our framework into the *Combinatorial Upper Confidence Bound (CUCB)* algorithm (Algorithm 1). To better handle the non-stationary rewards induced by ongoing flow training (Section above), we compute bandit statistics using a **sliding window** of the most recent H unrestricted evaluation rounds (i.e., the feedback obtained from GFLOWNET.GEN(ALL), aggregated every I rounds if interval aggregation is used). Concretely, for each arm i , we maintain a FIFO buffer \mathcal{B}_i that stores up to H most recent observed arm rewards X_i (Eq. 3); we then set $\hat{\mu}_i = \frac{1}{|\mathcal{B}_i|} \sum_{x \in \mathcal{B}_i} x$. The UCB-adjusted estimate is

$$\bar{\mu}_i = \hat{\mu}_i + \sqrt{\frac{3 \ln t}{2T_i}}, \quad (7)$$

where t is the round index. This estimate ensures a principled balance between exploration and exploitation. Aside from the CUCB algorithm, there exist several other CMAB algorithms, such as Combinatorial Thompson Sampling (CTS) (Wang & Chen, 2018) and Efficient Sampling for Combinatorial Bandits (ESCB) (Kveton et al., 2015). Our framework is algorithm-agnostic and works with other CMAB methods like CTS and ESCB.

Algorithm 1 integrates our framework with CUCB. To han-

Algorithm 1 Combinatorial Upper Confidence Bound (CUCB) with Flow Network

Maintain: \mathcal{B}_i : buffer of recent rewards for arm i ; $T_i = |\mathcal{B}_i|$: sample count; $\hat{\mu}_i$: empirical mean
Inputs: m : # base arms; K : super arm size; T : # training rounds; H : window size

- 1: // **Initialization:**
- 2: **while** $\exists i \in \{1, \dots, m\}$ with $T_i = 0$ **do**
- 3: GFLOWNET.TRAIN(ALL); Receive feedback from GFLOWNET.GEN(ALL)
- 4: Compute and update arm rewards $\{X_i\}, \mathcal{B}_i, T_i, \hat{\mu}_i$
- 5: **end while**
- 6: // **Main Loop:**
- 7: **for** $t = m \rightarrow T$ **do**
- 8: Compute UCB: $\bar{\mu}_i \leftarrow \hat{\mu}_i + \sqrt{\frac{3 \ln t}{2T_i}}$; Select $\mathbb{S} = \text{select}(\bar{\mu}_1, \dots, \bar{\mu}_m)$
- 9: GFLOWNET.TRAIN(\mathbb{S}); Receive feedback from GFLOWNET.GEN(ALL)
- 10: Compute and update arm rewards $\{X_i\}_{i \in \mathbb{S}}, \mathcal{B}_i, T_i, \hat{\mu}_i$
- 11: **end for**

dle non-stationary rewards from ongoing training, we use a **sliding window** of the H most recent evaluation rounds. The UCB estimate balances exploration and exploitation.

For super arm selection, we adopt a **co-occurrence weighted greedy strategy** (Kabbur et al., 2013). We maintain a matrix $W \in \mathbb{R}^{N \times N}$ where W_{ij} records reward-weighted co-occurrence of arms i and j :

$$W_{ij} \leftarrow (1 - \alpha)W_{ij} + \alpha \cdot \mathbf{1}[i, j \in x] \cdot r(x). \quad (8)$$

During selection, we choose the highest UCB arm as seed, then greedily add arms maximizing:

$$\text{score}(a|\mathbb{S}) = \bar{\mu}_a + \lambda \cdot \frac{1}{|\mathbb{S}|} \sum_{b \in \mathbb{S}} W_{ab}, \quad (9)$$

where λ balances individual quality and co-occurrence synergy. This favors arms with both high UCB and strong synergistic patterns.

5. Experiment

We experimented on 5 commonly used standard tasks. As baselines, we use Trajectory Balance (TB) (Malkin et al., 2022a), Sub-Trajectory Balance (SUBTB) (Madan et al., 2023), Detailed Balance (DB) (Jain et al., 2022; Malkin et al., 2022a), LSGFN (Kim et al., 2023), Teacher (Kim et al., 2024c) and QGFN (Lau et al., 2024). All experiments are conducted on NVIDIA Tesla A100 80GB GPUs. Our evaluation centers on four key research questions (RQs):

⌚ **RQ1. How is the quality of candidates generated by**

CMAB-GFN? ↗ RQ2. How diverse are the generated candidates? ↗ RQ3. Why CMAB algorithms work for GFlowNets? ↗ RQ4. How robust is the proposed method across different hyperparameters? For RQ3, we performed further analysis by reporting the empirical mean rewards of each base arm in the Bit Sequence Generation task. We also conducted ablation studies, replacing the CMAB framework with alternative strategies such as Hard Pruning and Proportional Pruning to assess their effects in Appendix G. We introduce a baseline called **RandGFN** in all experiments, which replaces CMAB with random pruning.

Computational Fairness. To ensure fair comparison, all methods are trained with the same number of rounds and receive the same number of training samples per round for gradient updates. While CMAB-GFN’s two-phase protocol incurs additional environment calls for CMAB arm selection (e.g., 100 evaluation samples vs. 400 training samples per round in our molecule experiments), these evaluation samples serve *exclusively* for arm selection and do *not* contribute to GFlowNet training. Consequently, all methods receive equivalent training signals, and the additional cost lies solely in reward evaluations. Wall-clock time and GPU memory consumption are reported in Appendix I, demonstrating that the evaluation overhead remains modest relative to the performance gains. Following standard practice in GFlowNet literature (Bengio et al., 2021; Malkin et al., 2022a), we assume access to an efficient reward function or proxy model that evaluates generated candidates at negligible cost.

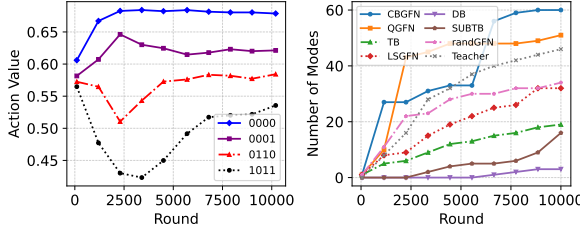


Figure 3. Experimental results on Bit Sequence task. Left panel shows how different action values change as the training progresses, where action values refer to the empirical mean rewards for each base arm, corresponding to $\hat{\mu}_i$ in Eq. 7. Right panel shows the mode discovered by different methods.

5.1. Bit Sequence Generation

5.1.1. TASK DEFINITION

The task is to generate binary bit sequences using the set $\{0, 1\}$ with a fixed length $n = 120$ with a terminal state space of $2^{120} \approx 10^{36}$ and more intermediate states. The reward of a terminal x is defined as $R(x) = \exp(-\min_{m \in M} \text{dist}(x, m))$, where $\text{dist}(x, m)$ is the Levenshtein Distance of two sequences following (Malkin et al., 2022a; Zhang et al., 2023b). M is a predefined sequence set

to be discovered as modes. The mode $m \in M$ is regarded as found if there exists a sample x satisfying $\text{dist}(x, m) < \delta$, where δ is a predefined parameter.

In this task, we consider a more complex version with many more intermediate states. Malkin et al. (2022a) considers the process as a left-to-right generation where the state space is only a simple tree. Lau et al. (2024); Shen et al. (2023) use a prepend-append MDP to induce a DAG. In our setting, instead of prepending or appending to the existing sequence, we first divide the sequence into $\lfloor \frac{n}{k} \rfloor$ positions. We can insert a generated k -bit into any unfilled position, resulting in a more complex DAG.

5.1.2. RESULT

The performance comparison of different methods on the bit sequence task is illustrated in Figure 3. GFlowNets employing TB objective demonstrate superior results, outperforming all other objective functions. CMAB-GFN successfully identifies all potential modes, representing a substantial advancement in mode discovery efficiency. Figure 3-a illustrates the evolution of μ_i for various base arms (actions). As training progresses with the CUCB algorithm’s action selection, the arms diverge, converging to distinct outcomes. Notably, the actions $\{0000, 1111\}$ emerge as the highest-scoring, aligning with the construction of M , where $\{0000, 1111\}$ appear most frequently compared to other actions.

5.2. Molecule Design

5.2.1. TASK DEFINITION

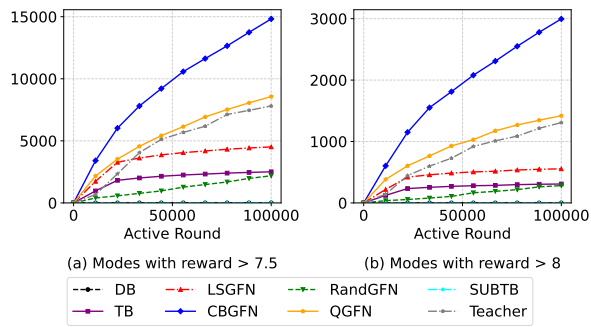


Figure 4. The curve of number of modes varying with rounds (10^3) on Molecule Design. Left panel shows the number of modes discovered with a reward $R > 7.5$. Right panel shows the number of modes discovered with a reward $R > 8$.

We consider the most common scenario for GFlowNets, the fragment-based molecule generation task. The objective is to design a variety of molecules with a high reward, where the reward is given by a proxy model predicting the binding affinity to the sEH (soluble epoxide hydrolase) protein based on a docking prediction (Trott & Olson, 2010). We use the proxy model provided by (Bengio et al., 2021).

Table 2. Comparison on Molecule Design. *Modes R>7.5/8* means the number of modes with a reward bigger than 7.5/8. *Top1000-perf* denotes the average reward of the best 1000 candidates. *Top1000-similarity* denotes the tanimoto similarity of the best 1000 candidates. Best result marks exclude results with less than 1000 discovered high-scoring modes.

Model	Modes R>7.5 \uparrow	Modes R>8 \uparrow	Top1000	
			Perf \uparrow	Similarity \downarrow
CMAB-GFN	14913	3207	8.436	0.49
QGFN	8567	1420	8.395	0.54
LSGFN	4514	555	8.316	0.53
TB	2507	308	8.233	0.47
SUBTB	6	0	7.245	0.50
DB	6	0	7.124	0.44
Teacher	7811	1308	8.364	0.49
RandGFN	2188	282	8.248	0.46

In this task, the states are represented as molecule graphs or SMILES. The action space consists of two components: selecting which molecular stems to extend and choosing which building blocks to add. The maximum number of allowed blocks controls the size of the state space. The vocabulary of building blocks consists of 105 distinct elements, where a block has several possible attachment points(stems). We generate a molecule graph of up to 8 fragments. Therefore, the terminal state space is more than $105^8 \approx 10^{16}$.

We define each block as a base arm and choose K blocks as a super arm. There are C_{105}^K different base arms. We use Tanimoto similarity (Bender & Glen, 2004) to distinguish different modes, with a threshold of 0.7. Furthermore, we conduct a comprehensive analysis to examine how different values of K affect the algorithm’s performance, particularly in terms of controlling its greediness.

5.2.2. RESULT

The comparative performance of various models is summarized in Table 2 and Figure 4. We observe that the baseline SUBTB consistently underperforms in both mode discovery and the generation of high-reward candidates. This pattern is not unique to our experiments; a similar trend was reported in the molecule design task by Lau et al. (2024), suggesting that SUBTB may face intrinsic challenges in effectively exploring complex reward landscapes. Our proposed CMAB-GFN demonstrates remarkable improvements in high-scoring mode discovery. During our experiments, the model successfully identified over 10,000 high-scoring modes ($R > 7.5$) with 100,000 training rounds. Furthermore, CMAB-GFN achieves superior performance in terms of average reward for the top 1000 candidates, outperforming all baseline methods.

Table 2 reports the Tanimoto similarity of the Top-1000 candidates. While sampling within a fixed pruned subspace can increase similarity by concentrating probability mass on a narrow region, our CMAB controller repeatedly re-

selects the super arm (Alg. 1, line 11), effectively mixing samples across different subspaces. As a result, CMAB-GFN achieves the best Top-1000 reward while keeping similarity competitive (0.49), substantially lower than other pruning-based baselines such as QGFN (0.54), suggesting that the gain in quality does not come from collapsing to near-duplicate candidates.

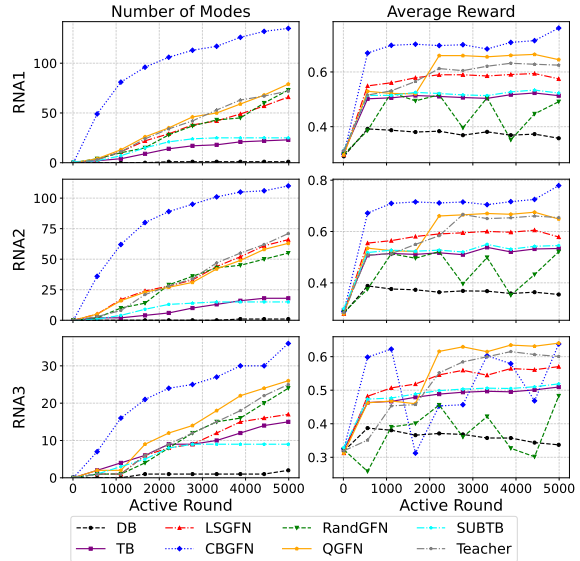


Figure 5. Performance comparison on RNA design tasks. Rows correspond to RNA-1, RNA-2, and RNA-3, respectively.

5.3. RNA-Binding

5.3.1. TASK DEFINITION

The task is to generate a string of 14 nucleobases. We use a prepend-append MDP to keep adding tokens to a string until it reaches the maximum length, following Kim et al. (2023). There are 4 tokens: adenine (A), cytosine (C), guanine (G), and uracil (U). We conducted experiments on three different target transcriptions: L14-RNA1, L14-RNA2, and L14-RNA3 proposed by Sinai et al. (2020). We treat each token as a base arm, and K is set to 2/3, denoting that we can either choose 2 base arms or 3 base arms as a super arm.

5.3.2. RESULT

Figure 5 reports the results on three RNA tasks, each evaluated by Number of Modes Discovered and Average Reward. CMAB-GFN consistently outperforms baselines: it discovers nearly twice as many modes as the strongest competitor and achieves higher average and Top-1000 rewards in Tasks 1 and 2, while remaining competitive in Task 3. The slight instability in Task 3 stems from averaging over only 10 rounds, during which the agent may explore subspaces with suboptimal rewards or insufficiently learned dynamics. We further analyze the impact of the reward exponent β (inverse

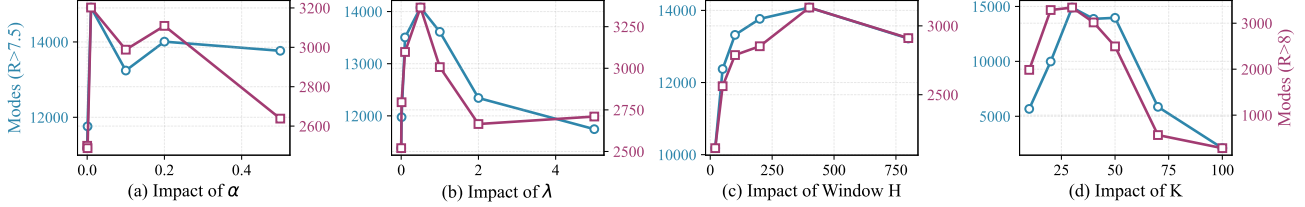


Figure 6. Ablation study on key hyperparameters. We evaluate sensitivity to super arm size K , co-occurrence update rate α , co-occurrence weighting coefficient λ , and sliding-window size H on the molecule generation task. Each panel shows the number of discovered modes ($R > 7.5$) and discovered modes ($R > 8$).

temperature) on RNA tasks in Section F.1.

5.4. Ablation Study and Sensitivity Analysis

Our CMAB-guided sampling introduces several key hyperparameters: the super arm size K , the co-occurrence update rate α (Eq. 10), the co-occurrence weighting coefficient λ (Eq. 11), and the sliding-window size H (Algorithm 1). To assess their impact, we conduct systematic ablation studies on the molecule generation task.

Figure 6 demonstrates that CMAB-GFN exhibits robust performance across reasonable hyperparameter ranges. **Super arm size K** is a fundamental parameter determining how many base arms are retained in each subspace. When K is too small (e.g., $K = 10$), the search space becomes overly constrained, limiting diversity and reducing the number of discovered high-reward modes. Conversely, when K is too large (e.g., $K = 100$), the subspace pruning becomes less effective, and the framework approaches the behavior of vanilla GFlowNets. Moderate values ($K \in [20, 50]$) strike an optimal balance, keeping the subspace sufficiently compact to guide exploration toward high-reward regions while preserving enough diversity to discover multiple distinct modes. **Co-occurrence update rate α** controls the smoothness of exponential moving averaging in W : moderate values ($\alpha \in [0.01, 0.1]$) maintain stable performance, while extreme values (0 or 0.2) show marginal degradation. **Co-occurrence weighting λ** interpolates between individual arm quality (UCB) and pairwise synergy (W): setting $\lambda = 0$ slightly underperforms, while moderate values (0.25–1.0) consistently improve performance by exploiting synergistic combinations. Excessively large λ (2.0) degrades results by over-emphasizing spurious correlations. **Sliding-window size H** balances bias and variance: very small windows ($H = 50$) suffer from high-variance estimates, while moderate windows ($H = 400$) maintain stable performance.

Overall, the method exhibits smooth performance surfaces with no brittle failure modes. Hyperparameter tuning primarily affects the speed and stability of bandit adaptation rather than qualitative behavior. For new tasks, we recommend K approximately 40–60% of the total number of base arms N , $\alpha \in [0.01, 0.1]$, $\lambda \in [0.25, 1.0]$, and H covering a

few hundred evaluation rounds as a robust starting point.

Table 3. Comparison of CMAB methods on molecule generation task. Results shown as percentages relative to CUCB baseline (100%).

Method	Modes $R > 7.5$	Modes $R > 8$	Top-K Reward
CUCB (baseline)	100.0%	100.0%	100.0%
CTS	93.5%	85.0%	99.9%
ESCB	103.8%	103.4%	100.1%

We conduct an additional experiment where we replaced CUCB with other CMAB algorithms. Table 3 reports the results as percentages relative to CUCB (baseline = 100%). All three methods achieve competitive performance, with ESCB showing slight improvements in mode discovery while CTS underperforms moderately.

6. Conclusion and Limitation

Conclusion: This paper proposes CMAB-GFN, a method designed to enhance the greediness of the sampling process while preserving the diversity of generated candidates. We begin by partitioning the entire state space into multiple subspaces. Next, we employ the CUCB algorithm to effectively balance exploration and exploitation and find the optimal subspaces. To address the challenges posed by narrow-deep network architectures, we propose techniques to transform them into more balanced wide-deep structures. Experimental results across various tasks demonstrate the effectiveness and efficiency of CMAB-GFN.

Limitations: Although our framework is theoretically applicable to tasks like listwise recommendation and combinatorial optimization problems, empirical validation on these tasks remains for future work. Another limitation of the proposed method is that it assumes a fixed reward distribution in the environment. In scenarios where the high-reward state space shifts during training, the benefits are limited and may even disappear.

References

Agarwal, M., Aggarwal, V., Umrawal, A. K., and Quinn, C. Dart: Adaptive accept reject algorithm for non-linear

combinatorial bandits. In *Proceedings of the AAAI Conference on Artificial Intelligence*, volume 35, pp. 6557–6565, 2021.

Bender, A. and Glen, R. C. Molecular similarity: a key technique in molecular informatics. *Organic & biomolecular chemistry*, 2(22):3204–3218, 2004.

Bengio, E., Jain, M., Korablyov, M., Precup, D., and Bengio, Y. Flow network based generative models for non-iterative diverse candidate generation. *Advances in Neural Information Processing Systems*, 34:27381–27394, 2021.

Chen, R., Wang, X., Hu, R., Li, Z., and Huang, L. Proxy-free gflownet. *arXiv preprint arXiv:2505.20110*, 2025.

Chen, W., Wang, Y., and Yuan, Y. Combinatorial multi-armed bandit: General framework and applications. In *International conference on machine learning*, pp. 151–159. PMLR, 2013.

Chen, W., Hu, W., Li, F., Li, J., Liu, Y., and Lu, P. Combinatorial multi-armed bandit with general reward functions. *Advances in Neural Information Processing Systems*, 29, 2016.

Chen, W., Wang, L., Zhao, H., and Zheng, K. Combinatorial semi-bandit in the non-stationary environment. In *Uncertainty in Artificial Intelligence*, pp. 865–875. PMLR, 2021.

Cretu, M., Harris, C., Igashov, I., Schneuing, A., Segler, M., Correia, B., Roy, J., Bengio, E., and Liò, P. Synflownet: Design of diverse and novel molecules with synthesis constraints. *arXiv preprint arXiv:2405.01155*, 2024.

Fourati, F., Alouini, M.-S., and Aggarwal, V. Federated combinatorial multi-agent multi-armed bandits. *arXiv preprint arXiv:2405.05950*, 2024a.

Fourati, F., Quinn, C. J., Alouini, M.-S., and Aggarwal, V. Combinatorial stochastic-greedy bandit. In *Proceedings of the AAAI Conference on Artificial Intelligence*, volume 38, pp. 12052–12060, 2024b.

Gao, G., Huang, H., Xiao, M., Wu, J., Sun, Y.-E., and Zhang, S. Auction-based combinatorial multi-armed bandit mechanisms with strategic arms. In *IEEE INFOCOM 2021-IEEE Conference on Computer Communications*, pp. 1–10. IEEE, 2021.

Hu, E. J., Jain, M., Elmoznino, E., Kaddar, Y., Lajoie, G., Bengio, Y., and Malkin, N. Amortizing intractable inference in large language models. *arXiv preprint arXiv:2310.04363*, 2023.

Hu, R., Zhang, Y., Li, Z., and Huang, L. Beyond squared error: Exploring loss design for enhanced training of generative flow networks. *arXiv preprint arXiv:2410.02596*, 2024.

Ikram, Z., Pan, L., and Liu, D. Evolution guided generative flow networks. *arXiv preprint arXiv:2402.02186*, 2024.

Jain, M., Bengio, E., Hernandez-Garcia, A., Rector-Brooks, J., Dossou, B. F., Ekbote, C. A., Fu, J., Zhang, T., Kulgour, M., Zhang, D., et al. Biological sequence design with gflownets. In *International Conference on Machine Learning*, pp. 9786–9801. PMLR, 2022.

Kabbur, S., Ning, X., and Karypis, G. Fism: factored item similarity models for top-n recommender systems. In *Proceedings of the 19th ACM SIGKDD international conference on Knowledge discovery and data mining*, pp. 659–667, 2013.

Kim, H., Kim, M., Choi, S., and Park, J. Genetic-guided gflownets for sample efficient molecular optimization. *arXiv preprint arXiv:2402.05961*, 2024a.

Kim, M., Yun, T., Bengio, E., Zhang, D., Bengio, Y., Ahn, S., and Park, J. Local search gflownets. *arXiv preprint arXiv:2310.02710*, 2023.

Kim, M., Choi, S., Kim, H., Son, J., Park, J., and Bengio, Y. Ant colony sampling with gflownets for combinatorial optimization. *arXiv preprint arXiv:2403.07041*, 2024b.

Kim, M., Choi, S., Yun, T., Bengio, E., Feng, L., Rector-Brooks, J., Ahn, S., Park, J., Malkin, N., and Bengio, Y. Adaptive teachers for amortized samplers. *arXiv preprint arXiv:2410.01432*, 2024c.

Kveton, B., Wen, Z., Ashkan, A., and Szepesvari, C. Tight regret bounds for stochastic combinatorial semi-bandits. In *Artificial Intelligence and Statistics*, pp. 535–543. PMLR, 2015.

Lau, E., Lu, S., Pan, L., Precup, D., and Bengio, E. Qgfn: Controllable greediness with action values. *Advances in neural information processing systems*, 37:81645–81676, 2024.

Madan, K., Rector-Brooks, J., Korablyov, M., Bengio, E., Jain, M., Nica, A. C., Bosc, T., Bengio, Y., and Malkin, N. Learning gflownets from partial episodes for improved convergence and stability. In *International Conference on Machine Learning*, pp. 23467–23483. PMLR, 2023.

Malkin, N., Jain, M., Bengio, E., Sun, C., and Bengio, Y. Trajectory balance: Improved credit assignment in gflownets. *Advances in Neural Information Processing Systems*, 35:5955–5967, 2022a.

Malkin, N., Lahlou, S., Deleu, T., Ji, X., Hu, E., Everett, K., Zhang, D., and Bengio, Y. Gflownets and variational inference. *arXiv preprint arXiv:2210.00580*, 2022b.

Rector-Brooks, J., Madan, K., Jain, M., Korablyov, M., Liu, C.-H., Chandar, S., Malkin, N., and Bengio, Y. Thompson sampling for improved exploration in gflownets. *arXiv preprint arXiv:2306.17693*, 2023.

Robbins, H. Some aspects of the sequential design of experiments. 1952.

Shen, M. W., Bengio, E., Hajiramezanali, E., Loukas, A., Cho, K., and Biancalani, T. Towards understanding and improving gflownet training. In *International conference on machine learning*, pp. 30956–30975. PMLR, 2023.

Silva, T., Alves, R. B., da Silva, E. d. S., Souza, A. H., Garg, V., Kaski, S., and Mesquita, D. When do gflownets learn the right distribution? In *The Thirteenth International Conference on Learning Representations*, 2025.

Sinai, S., Wang, R., Whatley, A., Slocum, S., Locane, E., and Kelsic, E. D. Adalead: A simple and robust adaptive greedy search algorithm for sequence design. *arXiv preprint arXiv:2010.02141*, 2020.

Slivkins, A. et al. Introduction to multi-armed bandits. *Foundations and Trends® in Machine Learning*, 12(1-2):1–286, 2019.

Trott, O. and Olson, A. J. Autodock vina: improving the speed and accuracy of docking with a new scoring function, efficient optimization, and multithreading. *Journal of computational chemistry*, 31(2):455–461, 2010.

Vemgal, N., Lau, E., and Precup, D. An empirical study of the effectiveness of using a replay buffer on mode discovery in gflownets. *arXiv preprint arXiv:2307.07674*, 2023.

Wang, S. and Chen, W. Thompson sampling for combinatorial semi-bandits. In *International Conference on Machine Learning*, pp. 5114–5122. PMLR, 2018.

Zhang, D., Malkin, N., Liu, Z., Volokhova, A., Courville, A., and Bengio, Y. Generative flow networks for discrete probabilistic modeling. In *International Conference on Machine Learning*, pp. 26412–26428. PMLR, 2022.

Zhang, D., Dai, H., Malkin, N., Courville, A. C., Bengio, Y., and Pan, L. Let the flows tell: Solving graph combinatorial problems with gflownets. *Advances in neural information processing systems*, 36:11952–11969, 2023a.

Zhang, D., Pan, L., Chen, R. T., Courville, A., and Bengio, Y. Distributional gflownets with quantile flows. *arXiv preprint arXiv:2302.05793*, 2023b.

Zhang, D. W., Rainone, C., Peschl, M., and Bondesan, R. Robust scheduling with gflownets. *arXiv preprint arXiv:2302.05446*, 2023c.

Zhu, Y., Wu, J., Hu, C., Yan, J., Hou, T., Wu, J., et al. Sample-efficient multi-objective molecular optimization with gflownets. *Advances in Neural Information Processing Systems*, 36:79667–79684, 2023.

A. LLM Usage Statement

We only use LLMs as a language optimization tool to polish sentences, improving their readability and fluency. The LLM did not contribute to the scientific ideas, algorithm design, or experimental setup. All substantive content, reasoning, and conclusions are entirely the product of the authors. We accept full responsibility for all content in the paper, including parts refined or corrected by the LLM, and affirm that no text generated by the LLM constitutes original scientific contributions attributed to it.

B. Theorem Proof

We first state the precondition required for our theoretical analysis.

Precondition. Exploration Guarantee The forward policy π_t maintains a minimum exploration probability $\epsilon > 0$ throughout training, i.e., for any valid transition $s \rightarrow s'$, we have $\pi_t(s'|s) \geq \epsilon/|\mathcal{A}_s|$, where $|\mathcal{A}_s|$ is the number of available actions at state s .

Then we establish the convergence of GFlowNet policies and subsequently the convergence of base arm reward distributions.

Remark B.1 (Scope of the theoretical claims). The trajectory balance (TB) objective is *consistent*: any exact solution of the TB equations induces the reward-proportional terminal distribution. However, for general function approximation (e.g., neural networks) and non-convex optimization, a global convergence guarantee of TB training is not established in full generality. Our analysis below therefore separates (i) TB consistency (a property of the optimum) from (ii) policy stabilization during training (an assumption that can hold when the TB loss plateaus and updates become small).

Lemma B.2 (TB Consistency (Zero-loss Implies Target Distribution)). *Assume the environment induces a finite DAG with initial state s_0 and terminal set \mathcal{X} , and let $P_F(\cdot|s; \theta)$ and $P_B(\cdot|s; \theta)$ be valid forward/backward transition kernels with full support. If the TB constraints hold for all trajectories $\tau = (s_0 \rightarrow \dots \rightarrow x)$, i.e.,*

$$Z_\theta \prod_t P_F(s_t|s_{t-1}; \theta) = R(x) \prod_t P_B(s_{t-1}|s_t; \theta), \quad (10)$$

equivalently $\mathcal{L}_{TB}(\theta) = 0$, then the induced terminal distribution satisfies $\pi_\theta(x) = \frac{R(x)}{\sum_{x' \in \mathcal{X}} R(x')}$.

$$\pi_\theta(x) = \frac{R(x)}{\sum_{x' \in \mathcal{X}} R(x')}. \quad (11)$$

Proof. Fix a terminal state $x \in \mathcal{X}$ and sum (10) over all forward trajectories ending at x . The left-hand side becomes

$$Z_\theta \sum_{\tau: s_0 \rightarrow x} \prod_t P_F(s_t|s_{t-1}; \theta) = Z_\theta \pi_\theta(x),$$

where $\pi_\theta(x)$ is the probability of sampling terminal x under the forward policy. The right-hand side becomes

$$R(x) \sum_{\tau: s_0 \rightarrow x} \prod_t P_B(s_{t-1}|s_t; \theta) = R(x),$$

since the backward kernel defines a valid stochastic process on the reversed DAG and the total probability of reaching s_0 from x by following P_B is 1 (i.e., the sum over all backward trajectories from x to s_0 equals 1). Hence $Z_\theta \pi_\theta(x) = R(x)$ for all x , and normalizing over \mathcal{X} yields $\pi_\theta(x) \propto R(x)$. This is the standard consistency property of TB (Bengio et al., 2021; Malkin et al., 2022a). \square

Lemma B.3 (Convergence of Sampling Distribution). *Assume the terminal distributions $\{\pi_t\}$ produced by training satisfy pointwise convergence $\pi_t(x) \rightarrow \pi_\infty(x)$ for all $x \in \mathcal{X}$, and that $\sum_{x \in \mathcal{X}_i} \pi_\infty(x) > 0$. For any base arm i , define the conditional sampling distribution $p_t(x|i) = \pi_t(x)/\sum_{x' \in \mathcal{X}_i} \pi_t(x')$. Then:*

$$\lim_{t \rightarrow \infty} \sum_{x \in \mathcal{X}_i} |p_t(x|i) - p_\infty(x|i)| = 0, \quad (12)$$

where $p_\infty(x|i) = \pi_\infty(x)/\sum_{x' \in \mathcal{X}_i} \pi_\infty(x')$. Moreover, if π_∞ satisfies the TB constraints (e.g., $\mathcal{L}_{TB}(\theta_t) \rightarrow 0$ so that $\pi_\infty = \pi^*$ as in Lemma B.2), then $p_\infty(\cdot|i) = p^*(\cdot|i)$.

Proof. Since \mathcal{X}_i is finite and $\pi_t(x) \rightarrow \pi_\infty(x)$ for each $x \in \mathcal{X}$, we have:

$$p_t(x|i) = \frac{\pi_t(x)}{\sum_{x' \in \mathcal{X}_i} \pi_t(x')} \xrightarrow{t \rightarrow \infty} \frac{\pi_\infty(x)}{\sum_{x' \in \mathcal{X}_i} \pi_\infty(x')} = p_\infty(x|i). \quad (13)$$

The convergence in total variation follows from the finiteness of \mathcal{X}_i and pointwise convergence. \square

Theorem 1. Assume (i) π_t converges pointwise to a limiting terminal distribution π_∞ (policy stabilization), and (ii) candidates in $C_{i,t}$ are sampled i.i.d. from $p_t(\cdot|i)$ at each round. Then the reward distribution of each base arm i converges to a stable distribution. Specifically, let

$$X_{i,t} = \frac{1}{|C_{i,t}|} \sum_{x \in C_{i,t}} r(x), \quad (14)$$

where $C_{i,t}$ is the set of n candidates sampled at round t that contain base arm i , and $r(x) = R(x)/R_{\max}$ is the normalized reward. Then $X_{i,t}$ converges in distribution to a random variable X_i^* as $t \rightarrow \infty$.

Proof. We establish the convergence through the following steps.

Step 1: Characterization of the Limiting Distribution.

At round t , candidates in $C_{i,t}$ are sampled i.i.d. from the distribution $p_t(\cdot|i)$ over \mathcal{X}_i . The empirical mean reward is:

$$X_{i,t} = \frac{1}{|C_{i,t}|} \sum_{x \in C_{i,t}} r(x). \quad (15)$$

Define the limiting expected reward under the stabilized (limiting) conditional distribution:

$$\mu_{i,\infty} = \sum_{x \in \mathcal{X}_i} p_\infty(x|i) \cdot r(x). \quad (16)$$

If additionally the TB constraints are solved asymptotically (e.g., $\mathcal{L}_{\text{TB}}(\theta_t) \rightarrow 0$ so that $\pi_\infty = \pi^*$), then $p_\infty(\cdot|i) = p^*(\cdot|i)$ and $\mu_{i,\infty} = \mu_i^*$.

Step 2: Convergence of Conditional Expectations.

Let $\mu_{i,t} = \mathbb{E}[r(X)|X \sim p_t(\cdot|i)] = \sum_{x \in \mathcal{X}_i} p_t(x|i) \cdot r(x)$ be the expected reward under the current sampling distribution. By Lemma B.3, $p_t(x|i) \rightarrow p_\infty(x|i)$ for all $x \in \mathcal{X}_i$. Since $r(x) \in [0, 1]$ is bounded, the dominated convergence theorem yields:

$$\mu_{i,t} = \sum_{x \in \mathcal{X}_i} p_t(x|i) \cdot r(x) \xrightarrow{t \rightarrow \infty} \sum_{x \in \mathcal{X}_i} p_\infty(x|i) \cdot r(x) = \mu_{i,\infty}. \quad (17)$$

Step 3: Convergence in Distribution.

For fixed t , given $n_t = |C_{i,t}|$ samples, the empirical mean $X_{i,t}$ has:

$$\mathbb{E}[X_{i,t}] = \mu_{i,t}, \quad \text{Var}(X_{i,t}) = \frac{\sigma_{i,t}^2}{n_t}, \quad (18)$$

where $\sigma_{i,t}^2 = \sum_{x \in \mathcal{X}_i} p_t(x|i)(r(x) - \mu_{i,t})^2$ is the variance under $p_t(\cdot|i)$.

We now show convergence in distribution. For any $\delta > 0$, by Chebyshev's inequality:

$$\mathbb{P}(|X_{i,t} - \mu_{i,t}| > \delta) \leq \frac{\sigma_{i,t}^2}{n_t \delta^2} \leq \frac{1}{4n_t \delta^2}, \quad (19)$$

where we used $\sigma_{i,t}^2 \leq 1/4$ since $r(x) \in [0, 1]$.

Let $\varepsilon > 0$ be arbitrary. Choose T large enough such that for all $t > T$: (i) $|\mu_{i,t} - \mu_{i,\infty}| < \varepsilon/2$ (by Step 2), and (ii) n_t is sufficiently large that $1/(4n_t \delta^2) < \varepsilon/2$ for $\delta = \varepsilon/2$. Then for $t > T$:

$$\mathbb{P}(|X_{i,t} - \mu_{i,\infty}| > \varepsilon) \leq \mathbb{P}(|X_{i,t} - \mu_{i,t}| > \varepsilon/2) + \mathbb{P}(|\mu_{i,t} - \mu_{i,\infty}| > \varepsilon/2) \quad (20)$$

$$< \varepsilon/2 + 0 = \varepsilon/2. \quad (21)$$

This shows $X_{i,t} \xrightarrow{p} \mu_{i,\infty}$. More generally, the distribution of $X_{i,t}$ converges to a distribution concentrated around $\mu_{i,\infty}$. In the large-sample regime where $n_t \rightarrow \infty$, by the Central Limit Theorem, $(X_{i,t} - \mu_{i,t})\sqrt{n_t} \xrightarrow{d} \mathcal{N}(0, \sigma_{i,\infty}^2)$, where $\sigma_{i,\infty}^2 = \sum_{x \in \mathcal{X}_i} p_\infty(x|i)(r(x) - \mu_{i,\infty})^2$.

Combining the convergence of $\mu_{i,t} \rightarrow \mu_{i,\infty}$ and $\sigma_{i,t}^2 \rightarrow \sigma_{i,\infty}^2$ with Slutsky's theorem, we conclude that $X_{i,t}$ converges in distribution to X_i^* concentrated around $\mu_{i,\infty}$ (e.g., approximately $\mathcal{N}(\mu_{i,\infty}, \sigma_{i,\infty}^2/n^*)$ for large fixed batch size n^*), or concentrates at $\mu_{i,\infty}$ as $n_t \rightarrow \infty$.

Step 4: Uniform Integrability (Optional Strengthening).

Since $r(x) \in [0, 1]$, we have $X_{i,t} \in [0, 1]$ uniformly, implying $\{X_{i,t}\}$ is uniformly integrable. Combined with convergence in probability, this yields $\mathbb{E}[X_{i,t}] \rightarrow \mu_{i,\infty}$, establishing convergence in L^1 as well.

This completes the proof of Theorem 1.

Theorem 2 (Asymptotic Approximate Distributional Invariance). Under the two-phase protocol (restricted training on \mathbb{S} , unrestricted evaluation on *ALL*), assume there exists a sequence $\delta_t \downarrow 0$ such that for any base arm a and any two super arms \mathbb{S}, \mathbb{S}' that could be used in Phase 1 at round t , the resulting evaluation-time conditional sampling distributions satisfy

$$\|p_t^{\mathbb{S}}(\cdot|a) - p_t^{\mathbb{S}'}(\cdot|a)\|_1 \leq \delta_t. \quad (22)$$

Then the distribution of the unrestricted evaluation reward estimate X_a^t becomes asymptotically invariant to the Phase 1 super arm, i.e., the CMAB “distributional consistency” assumption holds approximately in late training.

Proof. In Phase 2, X_a^t is an empirical average of bounded rewards (after normalization, $r(\cdot) \in [0, 1]$) over samples drawn from $p_t^{\mathbb{S}}(\cdot|a)$. For any bounded function f with $\|f\|_\infty \leq 1$, the difference in expectations is bounded by total variation:

$$|\mathbb{E}_{p_t^{\mathbb{S}}} [f] - \mathbb{E}_{p_t^{\mathbb{S}'}} [f]| \leq \frac{1}{2} \|p_t^{\mathbb{S}}(\cdot|a) - p_t^{\mathbb{S}'}(\cdot|a)\|_1 \leq \frac{1}{2} \delta_t.$$

Taking $f(x) = r(x)$ yields $|\mathbb{E}[X_a^t|\mathbb{S}] - \mathbb{E}[X_a^t|\mathbb{S}']| \leq \frac{1}{2} \delta_t$. Since $\delta_t \rightarrow 0$, the dependence of the evaluation-time arm statistics on the preceding training subspace vanishes asymptotically.

C. Regret Analysis

C.1. Regret Bound

The flow network evolves dynamically throughout training, resulting in time-varying reward distributions for each base arm i . While these distributions can stabilize in late training under policy-stabilization assumptions, the inherent non-stationarity introduces considerable uncertainty into the system. Such temporal variability presents significant challenges for deriving a precise regret bound for the learning algorithm.

However, we can still construct empirical regret metrics to evaluate algorithm performance. A practical approach is to use the best empirical arm observed up to time t , denoted as $\hat{\mu}_t(\mathbb{S}^*)$, as a proxy for the unknown optimal mean reward. The estimated cumulative regret is then computed as:

$$\hat{R}(T) = \sum_{t=1}^T (\hat{\mu}_t(\mathbb{S}^*) - \hat{\mu}_t(\mathbb{S})). \quad (23)$$

We employ the metric of empirical cumulative regret to quantify the performance gap between consistently selecting the currently known optimal super arm and the super arm chosen by our algorithm. To comprehensively evaluate our method’s efficacy in minimizing regret, we introduce a baseline random strategy called RandGFN that uniformly selects K base arms at each round.

Figure 7 presents the cumulative regret curves for CMAB-GFN and the RandGFN, revealing distinct performance differences across tasks:

1. Bit Sequence Generation Task (left panel): The random policy exhibits competitive performance, resulting in a moderate regret gap between the two models. This suggests that simple heuristics suffice in this simpler task setting.
2. Molecule Design Task (middle panel): CMAB-GFN demonstrates substantial improvement, achieving a significantly lower cumulative regret than RandGFN. This highlights the proposed model’s effectiveness in optimizing structured, complex objectives.

Table 4. Key hyperparameter setting in Bit Sequence Generation task

Parameter	Value
Batch size	16
Number of steps	10000
k-bits	4
Lamda	1.9
Learning rate	1e-3
Z Learning rate	1e-3
β	2
Explore Epsilon	0.01
K	4
Decision Interval	100

3. L14-RNA1 Task (right panel): The regret gap widens again, where CMAB-GFN substantially outperforms RandGFN, indicating its ability to handle intricate combinatorial challenges in nucleic acid sequence optimization.

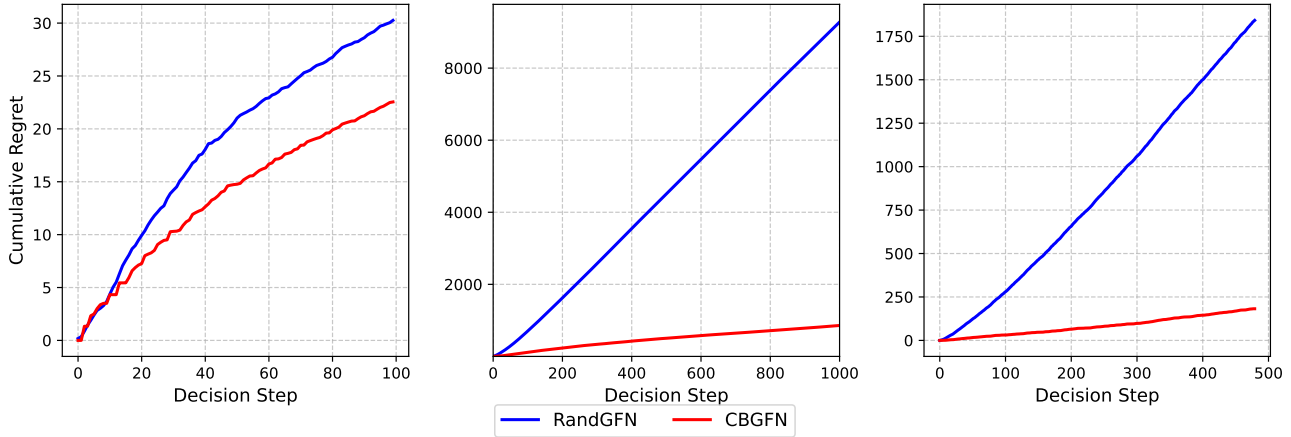


Figure 7. Experimental result on cumulative regret with different tasks. Left: Cumulative regret of models in Bit Sequence Generation Task. Center: Cumulative regret of models in Molecule Design Task. Right: Cumulative regret of models in L14-RNA1 Task.

D. Experiment details: Bit Sequence

Here we present the hyperparameter configuration for our bit sequence generation experiments (Table 4). While adopting the baseline framework from [Malkin et al. \(2022a\)](#), we reduce the training steps from 50,000 to 10,000. Each action is represented by $k = 4$ bits, and through empirical validation, we selected $K=4$ candidate arms from $\{2, 4, 6, 8, 10\}$. For the CMAB algorithm, we determined 100 steps to be the optimal decision interval after evaluating candidates from $\{50, 100, 200, 300, 400, 500\}$.

D.1. Optimal Super Arm Configuration

The set M is constructed through random combinations of substrings derived from the base patterns $\{00000000, 11111111, 11110000, 00001111, 00111100\}$. For the case where $K = 4$, we can analytically determine the optimal super arm configuration as $\mathbb{S} = \{0000, 1111, 1100, 0011\}$. This configuration enables perfect mode identification within its substate space, achieving an average distance of 0.0 to all target modes. We evaluate the performance when consistently selecting this optimal super arm configuration in Figure 8a.

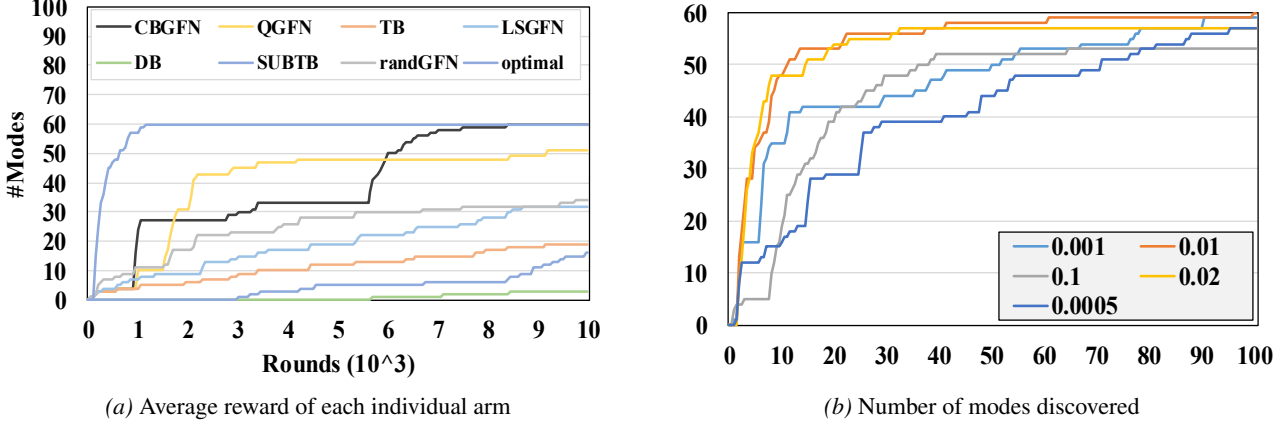


Figure 8. Supplementary Experimental Results for the Bit Sequence Task.

Table 5. Key hyperparameter setting in Molecule Design

Parameter	Value
Batch size	4
Number of steps	100000
Lamda	0.99
Learning rate	5e-4
Z Learning rate	5e-3
Tanimoto Similarity Threshold	0.7
β	8
Explore Epsilon	0.05
K	30
Decision Interval	400

D.2. Experiments on different ϵ

We conduct a systematic investigation of the exploration parameter ϵ , which controls the probability of random actions in the GFlowNets framework. This parameter critically influences the sampling behavior of the flow network within substate spaces. As shown in Figure 8b, through comprehensive testing across ϵ values $\{0.1, 0.01, 0.02, 0.001, 0.0005\}$, we find that $\epsilon = 0.01$ demonstrates superior performance in terms of mode discovery and sample quality.

The results indicate that moderate exploration ($\epsilon = 0.01$) achieves the best balance between exploration and exploitation, while higher values lead to excessive randomness and lower values result in insufficient exploration of the state space.

E. Experiment details: Molecule Design

We present the hyperparameter configurations for our Molecule Design Task experiments, as detailed in Table 5. Building upon the framework established by [Bengio et al. \(2021\)](#), we maintain their default parameter settings while introducing specific optimizations. After empirical evaluation, we set the number of base arms K to 30, selected from $\{8, 10, 20, 30, 40, 50, 60, 70, 80, 90, 100\}$, and determined the optimal decision interval for the CMAB algorithm to be 400 from $\{50, 100, 200, 300, 400, 500\}$.

F. Experiment details: RNA-Binding

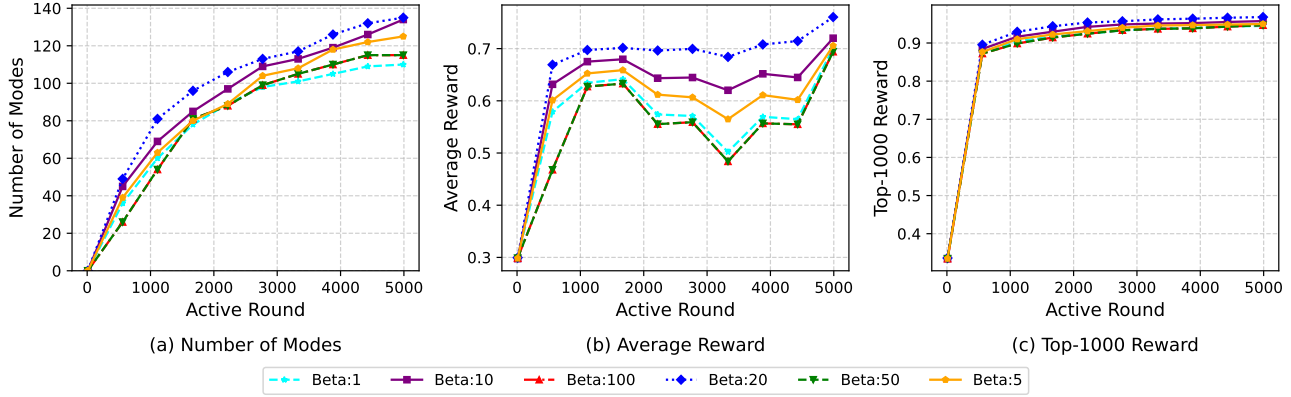
In this section, we give the hyperparameters used for each of our experiments' RNA-Binding Task as shown in Table 6. In our experimental setup, the learning rate of 1×10^{-4} is selected from $\{1 \times 10^{-5}, 1 \times 10^{-4}, 1 \times 10^{-3}, 5 \times 10^{-3}\}$ and the Z learning rate of 1×10^{-2} is selected from $\{1 \times 10^{-5}, 1 \times 10^{-4}, 1 \times 10^{-3}, 5 \times 10^{-3}\}$. The Lambda for SUBTB uses 0.9 out of $\{0.8, 0.9, 0.99, 0.999\}$. The explore epsilon is used to control the random action probability, five values

Table 6. Key hyperparameter setting in RNA-Binding task

Parameter	Value
Batch size	32
Number of steps	5000
RNA length	14
MDP style	Prepend and Append
Lamda	0.9
Learning rate	1e-4
Z Learning rate	1e-2
Mode metric	Hamming Ball 1
β	20
Explore Epsilon	0.01
K	2/3
Decision Interval	50

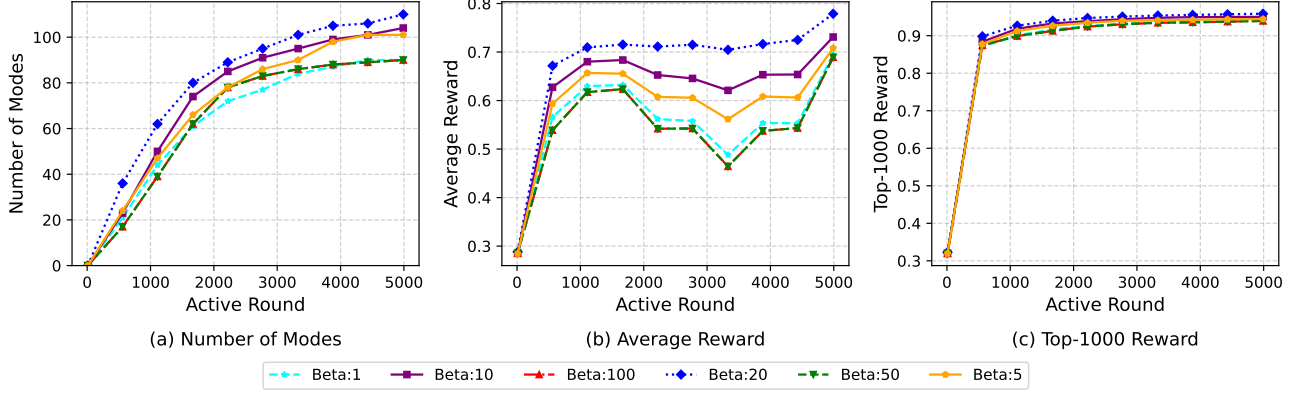
are tested, including $\{0.1, 0.01, 0.001, 0.0001, 0.0005\}$. We set the reward exponent β to 8 from $\{3, 4, 5, 6, 7, 8, 9, 10\}$. K is the number of base arms to compose the super arm selected from $\{1, 1/2, 2, 2/3, 3, 3/4, 4\}$, where $x/x + 1$ denotes we can choose x or $x + 1$ base arms as a super arm. Please note that the RNA1 environment we use is a little different from Teacher(Kim et al., 2024c). Our environment has 1590 modes in total, but Kim et al. (2024c) has 8967 modes. We replace the environment file of Teacher with our environment file to make a fair comparison. The environment is constructed following Kim et al. (2023).

F.1. Different settings: exponent β

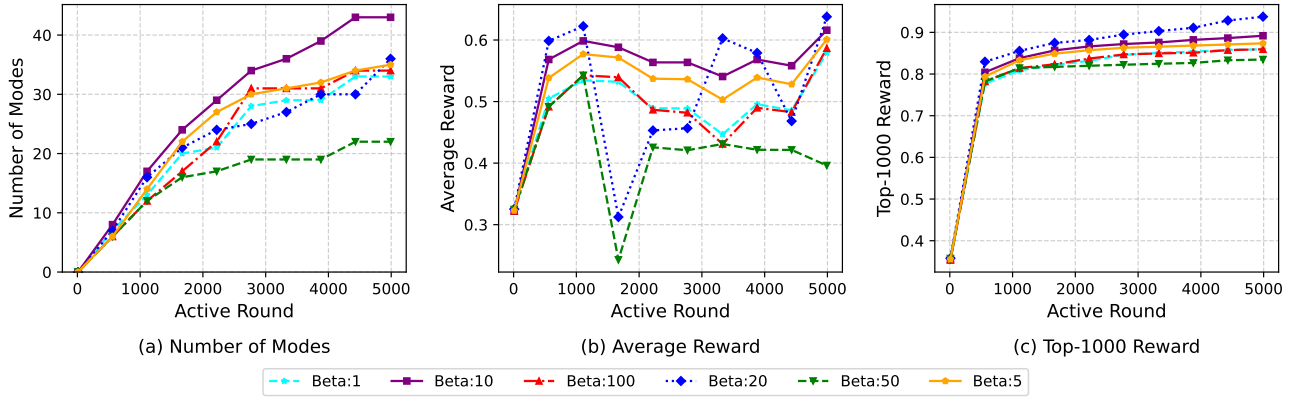

 Figure 9. Experimental result on RNA-Binding Task 1 with different β .

Since introduced by Bengio et al. (2021), there is already a useful technique to increase the greediness of GFlowNets, that is the exponent β . The adjusted reward function is formulated as $\hat{R}(x) = R(x)^\beta$. The higher β makes the model greedier but at the cost of greater numerical instability. Besides, since the middle-reward regions are adjusted into low-reward regions, the diversity is also reduced, leading to mode collapse (Lau et al., 2024). The choice of exponent β critically influences the behavior of the CUCB algorithm, as it directly modulates the reward scaling of individual arms. We experimented on different settings of exponent β as shown in Figure 9, Figure 10 and Figure 11.

In the L14-RNA1 task, models with varying β values consistently identified over 100 distinct modes, with the $\beta = 20$ configuration demonstrating superior performance compared to other settings. Notably, the model with $\beta = 1$ exhibited significantly poorer performance relative to other β values. Regarding average reward metrics, the $\beta = 20$ model achieved substantially better results, establishing a clear performance gap over other configurations. However, all models showed comparable performance when evaluating the top 1000 rewards.


 Figure 10. Experimental result on RNA-Binding Task 2 with different β .

In the L14-RNA2 task, while maintaining performance trends consistent with L14-RNA1, the task proved more challenging for mode discovery. All models identified fewer modes compared to L14-RNA1, yet the $\beta = 20$ configuration consistently demonstrated superior performance across all metrics, maintaining its lead over other parameter settings.


 Figure 11. Experimental result on RNA-Binding Task 3 with different β .

L14-RNA3 proves to be the most challenging task, exhibiting a significant decline in both discovered modes and average reward compared to other tasks. In this setting, $\beta = 10$ achieves the best overall performance, whereas $\beta = 20$, while attaining a higher average reward, suffers from instability. The task's difficulty suggests that using an excessively large β may be suboptimal, as it risks mode collapse by overly prioritizing high-reward candidates while neglecting mid-reward solutions.

G. Alternative strategies of super arms

Aside from top-K actions, we came up with three alternatives of arm selection: 1) selecting base arms proportional to their scores; 2) selecting base arms randomly; 3) keeping hard pruning but removing CMAB. Here, hard pruning refers to the permanent removal of some fixed actions from the selection pool. Random selection assigns equal selection probabilities to all base arms when constructing the super arm.

When employing a simple hard-pruning approach without the CMAB framework, GFlowNet initially discovers numerous high-reward modes quickly. However, the mode distribution within this constrained subspace is sparse, and after these easily accessible modes are found, the discovery rate drops significantly as the remaining modes become increasingly difficult to identify.

In contrast, a random selection strategy explores the space uniformly by choosing super arms indiscriminately, yielding

Table 7. Comparison of Different Methods in the molecule generation task.

Method	Modes $R > 7.5$	Modes $R > 8$	Top-1000 Reward	Top-1000 Similarity
Hard-Pruning	1069	132	7.95	0.47
Proportional	7554	1190	8.19	0.46
Random	2179	284	8.03	0.47
Top-K	12089	2952	8.31	0.49

Table 8. Profiling breakdown of runtime and memory consumption on Molecule Design (per 100 rounds).

Method	Sampling Time	Training Time	Update Time	Other Time	GPU Memory	CPU Memory
CBFlowNet (10^2)	61.07 s	308.90 s	0.03 s	151.9 s	4125.0 MB	2226.9 MB
CBFlowNet (10^4)	61.69 s	311.23 s	0.15 s	153.1 s	4148.3 MB	3051.2 MB
GFlowNet	50.70 s	310.64 s	0.00 s	153.7 s	4112.4 MB	2217.3 MB

an expected reward equal to the average across all sub-spaces. This approach achieves performance comparable to the Trajectory Balance (TB) method.

A proportional selection strategy, which chooses arms according to their estimated rewards, naturally outperforms random selection by favoring higher-reward regions. However, it remains less aggressive than the top-K approach. The proportional method discovers fewer total modes yet achieves marginally better performance in top-1000 similarity metrics. The results suggest that while proportional selection maintains better diversity, a more aggressive top- K strategy enables superior overall mode coverage.

H. Illustration of workflow

Here, we present a case study to illustrate how the proposed method work in the bit sequence generation task. The set M is constructed by randomly combining substrings derived from the base patterns 00000000, 11111111, 11110000, 00001111, 00111100. For $K = 4$, theoretical analysis reveals that the optimal super arm configuration is $S = 0000, 1111, 1100, 0011$, which achieves perfect mode identification within its substate space with an average distance of 0.0 to all target modes.

Initially, the base arm 0000 gradually gains higher values (as shown in Figure 3), leading to a suboptimal super arm configuration $S = 0000, 1111, 1100, 0001$. The UCB mechanism in line 11 of Algorithm 1 then identifies 0011 as a promising alternative - while its current estimated value is slightly lower than 0001, its higher uncertainty (due to insufficient exploration) suggests significant potential. This triggers an exploration phase where the algorithm selects $S = 0000, 1111, 1100, 0011$ as the new super arm. Subsequent evaluations confirm that 0011 consistently generates higher-quality candidates, and the value update in line 15 of Algorithm 1 reinforces its estimate in future rounds.

Notably, even though we know a priori that S is optimal, the CMAB framework continues to explore alternative subspaces with some probability. This characteristic ensures the algorithm maintains the capability to discover potentially better configurations while predominantly exploiting the known optimal solution, effectively balancing the exploration-exploitation trade-off throughout the learning process.

I. Time and GPU Memory Consumption

Table 8 reports a more fine-grained profiling breakdown of runtime and memory consumption in the molecule generation task, comparing vanilla GFlowNet and CBFlowNet under different arm size K ($10^2, 10^4$), where the parenthetical indicates the scale of bandit bookkeeping in our implementation (larger values imply heavier update workload). Overall, **training time dominates and is nearly identical across methods** (~ 311 s / 100 rounds), indicating that CBFlowNet introduces minimal overhead in network optimization. The extra cost mainly comes from **sampling time**, while the **update time** remains negligible but increases slightly as the setting grows. Memory footprints are comparable: GPU memory increases mildly (about +13–52 MB) and CPU memory by at most ~ 850 MB in our profiling.

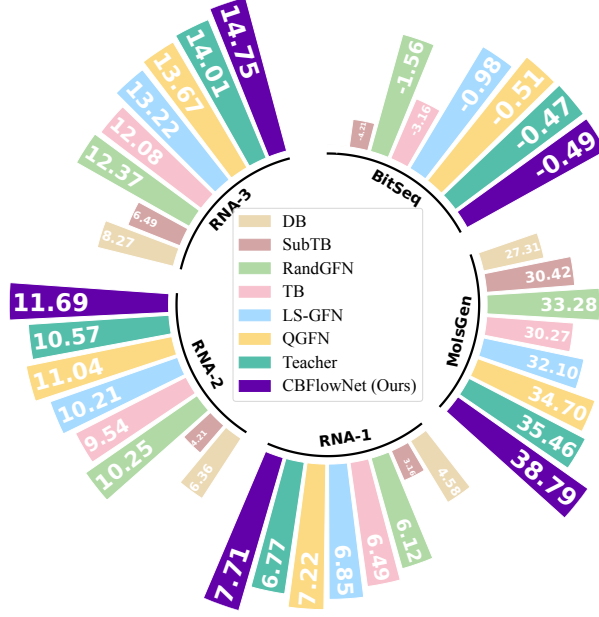


Figure 12. Experiment results on ELBO.

J. Evidence Lower Bound (ELBO)

We evaluate the goodness of fit to the target distribution using the evidence lower bound (ELBO) introduced by Kim et al. (2024c). ELBO is estimated by sampling M candidates and averaging the estimated $\log Z$ through a transformed TB objective:

$$Z \prod_{t=1}^n P_F(s_t|s_{t-1}) = F(X) \prod_{t=1}^n P_B(s_{t-1}|s_t). \quad (24)$$

The corresponding ELBO is approximated as:

$$ELBO \approx \frac{1}{M} \sum_{i=1}^M \left(\log R(x_i) + \sum_{t=1}^{n_i} P_B(s_{t-1}|s_t) - \sum_{t=1}^{n_i} P_F(s_t|s_{t-1}) \right), \quad (25)$$

where n_i is the length of the trajectory that generates terminal state x_i . Results are presented in Figure 12. The proposed CMAB-GFN achieves slightly better performance than the baselines, with Teacher remaining the strongest competitor.

K. Scalability

We show that the proposed method scales effectively to larger action spaces both theoretically and empirically. When selecting K arms from N total base arms to form a super arm, the accuracy of reward estimates $\hat{\mu}_i$ typically requires more rounds to converge as N grows. However, in practice, K often scales proportionally with N —for example, setting $K = 0.1N$ (selecting 10% of base arms). Under this scheme, the estimation accuracy of $\hat{\mu}_i$ remains stable with respect to N , leading to a fixed convergence rate.

Moreover, the computation of rewards $\hat{\mu}_i$ can be embedded within the flow-matching updates at negligible cost. Since our algorithm is heuristic, the additional computational burden is minimal, as also indicated in Table 8.

To further validate scalability, we experimented with enlarged action spaces. The molecule design task originally contains 105 building blocks with several stems each. By combining two actions into one base arm, the action space increases to $105 \times 105 = 11025$, denoted as CMAB-GFN (CA). As shown in Table 9, CMAB-GFN (CA) exhibits comparable or slightly better performance in discovering high-reward modes while incurring only negligible computational overhead.

Table 9. Performance comparison of different methods.

Method	Training Round	Modes $R > 7.5$	Modes $R > 8$	Top-1000 Reward	Top-1000 Similarity	Time (s / 100 rounds)
TB-GFN	10^5	1915	233	8.01	0.47	24.37
CMAB-GFN	10^5	12089	2952	8.31	0.49	27.95
CMAB-GFN (CA)	10^5	12433	2520	8.29	0.50	28.73

L. Experiments with Large Language Model Task

We also report experiments on a task with dynamic reward distributions (see Section 6) as a limitation study. Following [Hu et al. \(2023\)](#), we considered a subjectivity classification task where each movie review is labeled as either objective or subjective. This task is particularly challenging, as it involves both the E-step and M-step of the EM algorithm, with GFlowNet serving as the inference model in the E-step.

We adopt the default settings from the public implementation of [Hu et al. \(2023\)](#). For fine-tuning, we tested both GPT-2 and GPT-J 6B backbones.

Table 10. Comparison of CMAB-GFN and GFlowNet under GPT-2 and GPT-J backbones with different sample sizes. Results are reported as mean \pm standard deviation.

Method	GPT-2			GPT-J 6B		
	10 Samples	20 Samples	50 Samples	10 Samples	20 Samples	50 Samples
CMAB-GFN	0.59 ± 0.02	0.63 ± 0.03	0.78 ± 0.02	0.71 ± 0.02	0.83 ± 0.01	0.90 ± 0.01
GFlowNet	0.58 ± 0.03	0.61 ± 0.02	0.75 ± 0.03	0.71 ± 0.02	0.81 ± 0.02	0.87 ± 0.02

The results in Table 10 show that CMAB-GFN marginally outperforms GFlowNet in test accuracy across all training sample sizes. However, this task highlights a limitation of CMAB-GFN. The reward of a terminal state Z , defined as $p_{LM}(Z, Y | X)$, depends on both the label Y and input X . For instance, the word *factual* may yield a high reward when the label is “objective” but a low reward when the label is “subjective.” Thus, the high-reward state space shifts during training, which differs fundamentally from our original setting.

We categorize base arms into four groups: A) high-scoring under “objective” and low-scoring under “subjective”; B) high-scoring under “subjective” and low-scoring under “objective”; C) consistently high-scoring; D) consistently low-scoring.

Our framework is primarily designed to identify and filter arms of type D while retaining type C. In this dynamic setting, where types A and B fluctuate, we increased the base-arm set size K to ensure sufficient coverage of relevant arms (types A, B, and D).